



**HAL**  
open science

## Unexpectedly rapid aerosol formation in the Hunga Tonga plume

Elizabeth Asher, Michael Todt, Karen Rosenlof, Troy Thornberry, Ru-Shan Gao, Ghassan Taha, Paul Walter, Sergio Alvarez, James Flynn, Sean Davis, et al.

► **To cite this version:**

Elizabeth Asher, Michael Todt, Karen Rosenlof, Troy Thornberry, Ru-Shan Gao, et al.. Unexpectedly rapid aerosol formation in the Hunga Tonga plume. *Proceedings of the National Academy of Sciences of the United States of America*, 2023, 120 (46), 10.1073/pnas.2219547120 . hal-04301363

**HAL Id: hal-04301363**

**<https://hal.univ-reunion.fr/hal-04301363>**

Submitted on 24 Nov 2023

**HAL** is a multi-disciplinary open access archive for the deposit and dissemination of scientific research documents, whether they are published or not. The documents may come from teaching and research institutions in France or abroad, or from public or private research centers.

L'archive ouverte pluridisciplinaire **HAL**, est destinée au dépôt et à la diffusion de documents scientifiques de niveau recherche, publiés ou non, émanant des établissements d'enseignement et de recherche français ou étrangers, des laboratoires publics ou privés.

# Unexpectedly rapid aerosol formation in the Hunga Tonga plume

Elizabeth Asher<sup>1,2a\*</sup>, Michael Todt<sup>1,2b</sup>, Karen Rosenlof<sup>2</sup>, Troy Thornberry<sup>2</sup>, RuShan Gao<sup>2</sup>, Ghassan Taha<sup>3,4</sup>, Paul Walter<sup>5</sup>, Sergio Alvarez<sup>6</sup>, James Flynn<sup>6</sup>, Sean Davis<sup>2</sup>, Stephanie Evan<sup>7</sup>, Jerome Brioude<sup>7</sup>, Jean-Marc Metzger<sup>8</sup>, Dale F. Hurst<sup>1,9</sup>, Emrys Hall<sup>1,9</sup>, Kensy Xiong<sup>1,9</sup>

Elizabeth Asher [easher@noaa.gov](mailto:easher@noaa.gov)

Michael Todt [michael.todt@colorado.edu](mailto:michael.todt@colorado.edu)

Karen Rosenlof [karen.h.rosenlof@noaa.gov](mailto:karen.h.rosenlof@noaa.gov)

Troy Thornberry [troy.thornberry@noaa.gov](mailto:troy.thornberry@noaa.gov)

RuShan Gao [rushan.gao@noaa.gov](mailto:rushan.gao@noaa.gov)

Ghassan Taha [ghassan.taha-1@nasa.gov](mailto:ghassan.taha-1@nasa.gov)

Paul Walter [pauljw@stedwards.edu](mailto:pauljw@stedwards.edu)

Sergio Alvarez [slalvare@central.uh.edu](mailto:slalvare@central.uh.edu)

James Flynn [jhflynn@central.uh.edu](mailto:jhflynn@central.uh.edu)

Sean Davis [Sean.M.Davis@noaa.gov](mailto:Sean.M.Davis@noaa.gov)

Stephanie Evan [stephanie.evan@univ-reunion.fr](mailto:stephanie.evan@univ-reunion.fr)

Jerome Brioude [jerome.brioude@univ-reunion.fr](mailto:jerome.brioude@univ-reunion.fr)

Jean-Marc Metzger [jean-marc.metzger@univ-reunion.fr](mailto:jean-marc.metzger@univ-reunion.fr)

Dale F. Hurst [dale.hurst@noaa.gov](mailto:dale.hurst@noaa.gov)

Emrys Hall [Emrys.Hall@noaa.gov](mailto:Emrys.Hall@noaa.gov)

Kensy Xiong [kensy.xiong@noaa.gov](mailto:kensy.xiong@noaa.gov)

<sup>1</sup> Cooperative Institute for Research in Environmental Sciences, University of Colorado Boulder, 216 UCB, Boulder, CO 80309, United States

<sup>2</sup> NOAA Chemical Sciences Laboratory, 325 Broadway, Boulder, CO 80305, United States

<sup>3</sup> Morgan State University, 1700 East Cold Spring Lane McMechen Hall Rm 635, Baltimore, MD 21251, United States

<sup>4</sup> NASA Goddard Space Flight Center, 8800 Greenbelt Rd, Greenbelt, MD 20771, United States

<sup>5</sup> St. Edward's University, 3001 South congress, Austin, TX 78704, United States

<sup>6</sup> University of Houston, 4800 Calhoun Rd, Houston, TX 77004, United States

<sup>7</sup> Laboratoire de l'Atmosphère et des Cyclones (LACy), UMR8105, CNRS, Université de La Réunion, Saint-Denis, France

<sup>8</sup> Observatoire des Sciences de l'Univers de la Réunion, UAR 3365 (CNRS, Université de la Réunion, Météo-France), Saint-Denis, France

<sup>9</sup> NOAA Global Monitoring Laboratory, 325 Broadway, Boulder, CO 80305, United States

<sup>a</sup> Now at: NOAA Global Monitoring Laboratory

<sup>b</sup> Now at: Finnish Meteorological Institute (FMI), Helsinki, Finland

\*Corresponding author

**Classification:** Physical Sciences, Atmospheric Sciences

**Keywords:** stratospheric aerosol, rapid aerosol formation, SO<sub>2</sub>, volcanic plume, Hunga Tonga eruption

47 **Abstract**

48 The Hunga Tonga-Hunga Ha'apai (HT-HH) volcanic eruptions on Jan. 13 and 15, 2022  
49 produced a plume with the highest signal in stratospheric aerosol optical depth observed since  
50 the eruption of Mt. Pinatubo in 1991. Suites of balloon-borne instruments on a series of launches  
51 from Réunion Island intercepted the HT-HH plume within two weeks of the eruptions, yielding  
52 observations of the aerosol number and size distribution, and sulfur dioxide (SO<sub>2</sub>) and water  
53 vapor (H<sub>2</sub>O) concentrations. The measurements reveal an unexpected abundance of large  
54 particles in the plume, constrain the total sulfur injected to approximately 0.20 Tg, provide  
55 information on the altitude of the injection, and indicate that the formation of sulfuric acid  
56 aerosol was complete within three weeks. Large H<sub>2</sub>O enhancements contributed as much as  
57 ~30% to ambient aerosol surface area and likely accelerated SO<sub>2</sub> oxidation and aerosol formation  
58 rates in the plume to ~ 3 times faster than under normal stratospheric conditions.

59  
60 **Significance Statement**

61 Large volcanic eruptions can play an important role in Earth's radiative balance through  
62 stratospheric injections of sulfur dioxide that form sulfate aerosol. Here, we show that in situ  
63 observations are critical to constrain the injection mass of stratospheric sulfur and the  
64 stratospheric lifetime of sulfur dioxide. Such information is needed to better represent aerosol  
65 microphysics and improve predictions of the impacts of natural (or potentially anthropogenic)  
66 sulfur dioxide injections. Measurements in the fresh volcanic Hunga Tonga-Hunga Ha'apai  
67 plume in January 2022 revealed that stratospheric aerosol formation ended ~3 times faster than is  
68 typical in the presence of a large amount of water vapor, resulting in a high signal in aerosol  
69 extinction from an abundance of large particles.

70  
71  
72

73 **Main**

74 Volcanic plumes that reach the stratosphere can influence Earth's radiative balance and  
75 are a significant driver of climate variability (1). Under background conditions, sustaining the  
76 stratospheric aerosol burden requires the addition of  $\sim 0.1$  Tg sulfur (S)  $\text{yr}^{-1}$  from the oxidation of  
77 carbonyl sulfide and sulfur dioxide ( $\text{SO}_2$ ) (2), while stratospheric transport (3) and a variety of  
78 localized aerosol processes (4) contribute to heterogeneity in aerosol number and size.  
79 Simulating an eruption's impact on stratospheric aerosol requires either knowledge or  
80 assumptions of its injection height and mass (5), plume composition, location, and atmospheric  
81 state. In situ measurements within one to three weeks of an eruption can provide critical  
82 information for improving these assumptions.

83 The energetic eruption of the underwater Hunga Tonga-Hunga Ha'apai (HT-HH) volcano  
84 ( $20.54^\circ\text{S}$ ,  $175.38^\circ\text{W}$ ) on Jan. 15 (04:00 UTC) (6), together with a smaller eruption on Jan. 13  
85 (15:20 UTC), injected an estimated 150 Tg water vapor ( $\text{H}_2\text{O}$ ) (7) and  $0.41 \pm 0.01$  Tg  $\text{SO}_2$  into  
86 the stratosphere (7, 8). The combination of its explosivity and the extraordinary amount of  $\text{H}_2\text{O}$   
87 injected into the stratosphere make the Jan. 15 eruption unique in the satellite era. Estimated  
88 injection heights for these two eruptions ranged from 20 km on Jan. 13 to  $> 30$  km on Jan. 15,  
89 and the  $\text{SO}_2$  plumes quickly overlapped, making them difficult to distinguish (8). Radiosonde  
90 measurements reveal enhanced  $\text{H}_2\text{O}$  between 19 km and the maximum altitude of balloon  
91 soundings, near 30 km (9). The HT-HH aerosol layer generated the highest signal in  
92 stratospheric aerosol optical extinction since the eruption of Mt. Pinatubo in 1991 (10). Given the  
93 relatively small injections of  $\text{SO}_2$  (7, 8) by the HT-HH eruptions, the large signal in aerosol  
94 extinction sparked questions regarding the initial S injection (11), the role of  $\text{H}_2\text{O}$  in rapid  
95 aerosol formation in this plume and its timeline (12, 13).

96 In situ observations of particle number concentration and size distribution complement  
97 space-based aerosol retrievals. For the first three months after the HT-HH eruption, the Ozone  
98 Mapping and Profiler Suite-Limb Profile (OMPS-LP) sensor onboard the Suomi National Polar-  
99 orbiting Partnership (S-NPP) satellite supplied a continuous global record of the main volcanic  
100 plume's altitude between 16 – 30 km, its horizontal extent and its impact on stratospheric aerosol  
101 optical depth (sAOD) (10). The Tonga volcano Rapid Response Experiment ( $\text{TR}^2\text{Ex}$ ) provided  
102 high-resolution vertical profiles with relatively low uncertainty of  $\text{SO}_2$  (14) and  $\text{H}_2\text{O}$  (15, 16) to  
103  $\sim 30$  km altitude and information on the aerosol size distribution in the main plume, which  
104 cannot be reliably inferred from either satellite or ground-based measurements. Here, we  
105 leverage a combination of these in situ measurements and OMPS-LP retrievals (17) to address  
106 questions regarding the HT-HH eruption's impact on the lifetime of  $\text{SO}_2$  and the magnitude and  
107 altitude of the initial sulfur injection.

108

109

110 **Results**

111 1. Rapid Response Insights

112  $\text{TR}^2\text{Ex}$  was a unique deployment of a suite of balloon-borne instrumentation that  
113 repeatedly analyzed the composition of the volcanic plume 7 – 10 days after the second, larger  
114 HT-HH eruption. Sampling the fresh HT-HH plume yielded in situ observations of aerosol size  
115 distribution,  $\text{SO}_2$ , and  $\text{H}_2\text{O}$  at several pivotal times during its evolution (see Methods, Section 1  
116 for details; Table S1). In situ measurements from this campaign allow us to quantify the S  
117 gas/particle phase partitioning within the plume, study the vertical distribution of the S injection,

118 and explore the role of stratospheric H<sub>2</sub>O enhancements in increasing ambient aerosol size and  
119 extinction.

120 Portable Optical Particle Spectrometer (POPS) (18) measurements during TR<sup>2</sup>Ex show  
121 the impact of the HT-HH eruption on aerosol dry mass and extinction (enhancements ranged  
122 from two to three orders of magnitude), driven by high concentrations of large accumulation  
123 mode aerosols in the volcanic plume (Fig. 1; see Methods, Section 2 for details). By the time the  
124 plume reached La Réunion seven days after the second eruption, wind shear had stretched the  
125 initial injection into a thin slanted layer of varying thickness as it moved west (19). Positive  
126 altitude gradients in easterly windspeeds resulted in progressively shorter transit times with  
127 increasing altitude. TR<sup>2</sup>Ex instruments were unable to measure two isolated optically thin  
128 volcanic aerosol layer segments detected above 30 km by space-based and ground-based remote  
129 sensing instruments (10, 19)— as these were above the operation ceiling of balloon sondes. Parts  
130 of the aerosol layer between 25 km and 28 km (Fig. 1c-d) corresponded to a region with a  
131 substantial H<sub>2</sub>O enhancement (Fig. S1). Particle number concentration of both large and small  
132 particles (up to 1.5 μm) was as much as three orders of magnitude higher than in unperturbed air  
133 masses. The mode of the size distribution occurred at ~ 560 nm diameter, and the aerosol  
134 effective radius exceeded 0.3 μm (Fig. S2). With H<sub>2</sub>O enhancements of ~340 ppmv in this part  
135 of the plume, H<sub>2</sub>O contributed ~ 15% to the aerosol diameter at ~ 560 nm and ~ 30% to the total  
136 aerosol surface area (Fig. S3; see Methods, Section 2). Differences in aerosol surface area impact  
137 both extinction and stratospheric chemistry (20), highlighting the importance of calculating  
138 ambient aerosol size related to the HT-HH eruption. The air was much drier (< 17 ppmv H<sub>2</sub>O) in  
139 the part of the plume below 25 km, which contained an elevated number concentration of  
140 particles < 700 nm in diameter. The highest number concentration below 25 km occurred at the  
141 smallest particle size (Fig. 1e-f), and the aerosol effective radius was not noticeably different  
142 from baseline values (~ 0.2 μm; Fig. S2). Larger particles appeared more often in the wetter,  
143 higher altitude parts of the aerosol layer, presumably due to shorter SO<sub>2</sub> lifetimes and particle  
144 coagulation within the plume (12).

145 On three occasions, simultaneous in situ measurements of SO<sub>2</sub> and aerosol in the volcanic  
146 plume reveal varying rates of aerosol formation. Particles in the plume are presumed to be  
147 composed of sulfuric acid (H<sub>2</sub>SO<sub>4</sub>) formed from SO<sub>2</sub> oxidation and are designated estimated  
148 H<sub>2</sub>SO<sub>4</sub> (eH<sub>2</sub>SO<sub>4</sub>) (see Methods, Section 2 for details). Comparisons are shown between the mass  
149 mixing ratios of S in eH<sub>2</sub>SO<sub>4</sub> and SO<sub>2</sub> (Fig. 2a-c). The altitudes of SO<sub>2</sub> enhancements and aerosol  
150 accumulations correspond well, and the mass mixing ratios of S in eH<sub>2</sub>SO<sub>4</sub> exceeded those of S  
151 in SO<sub>2</sub> on two of three flights. Outside of the fresh HT-HH plume, the SO<sub>2</sub> partial pressure was  
152 below the detection limit of the SO<sub>2</sub> sonde. If SO<sub>2</sub> gas phase oxidation had proceeded at its  
153 typical rate (i.e., an e-folding stratospheric lifetime, τ<sub>strat</sub> = ~ 30 days) (21) after the two HT-HH  
154 eruptions, we would expect a ≤30% estimated H<sub>2</sub>SO<sub>4</sub> (eH<sub>2</sub>SO<sub>4</sub>) aerosol to ≥70% SO<sub>2</sub> split (by S  
155 mass) on Jan. 25, ~ 10.5 days after the second, larger eruption. In the wetter, higher altitude  
156 region of the plume, measured on Jan. 22, eH<sub>2</sub>SO<sub>4</sub> aerosol accounted for 90% of the total S in the  
157 plume (Fig. 2d), implying a τ<sub>strat</sub> = ~ 3 days. In a drier part of the aerosol layer encountered on  
158 Jan. 24 at 22 km, eH<sub>2</sub>SO<sub>4</sub> aerosol constituted 68% of the total S (τ<sub>strat</sub> = ~ 8 days), and on Jan. 25  
159 at 20 km, only 35% of the total S (τ<sub>strat</sub> = ~ 24 days). We infer that SO<sub>2</sub> oxidation in the fresh  
160 plume proceeded at different rates as a function of H<sub>2</sub>O, namely more quickly where H<sub>2</sub>O mixing  
161 ratios were higher due to an increased concentration of hydroxyl radicals (22, 23). These  
162 measurements also provide information on the vertical distribution of the S injection (i.e., the  
163 sum of the S in both SO<sub>2</sub> and in eH<sub>2</sub>SO<sub>4</sub> aerosol; Fig. 2d). The total S column mass of the higher

164 altitude part of the plume measured on Jan. 22 was nearly four times that of the lower altitude  
165 part of the plume measured on Jan. 24 and 25, suggesting that the majority of SO<sub>2</sub> was injected  
166 above 25 km (Fig. 2d).

## 167 168 2. Aerosol burden and stratospheric lifetime ( $\tau_{\text{strat}}$ ) of SO<sub>2</sub>

169 Quantifying the S burden in the tropical HT-HH aerosol layer helps constrain the  
170 stratospheric S injection and the  $\tau_{\text{strat}}$  of SO<sub>2</sub>, which are critical for model validation and have  
171 widespread implications for stratospheric chemistry. The calculation relies on the relationship  
172 between the aerosol S column and sAOD calculated using POPS size distributions on launches  
173 from La Réunion and on OMPS-LP retrievals of sAOD (see Methods, Section 3). As the plume  
174 moved westwards, TR<sup>2</sup>Ex launches sampled its core on Jan. 22 – 23 and trailing edge on Jan. 24  
175 – 25 (Fig. 3). The S in the eH<sub>2</sub>SO<sub>4</sub> aerosol layer grew from 0.03 Tg S on Jan. 18 to 0.15 Tg S on  
176 Jan. 26 and reached a maximum of 0.18 Tg S on Feb. 3 (Fig. 4a). We estimate that on Jan. 23, ~  
177 3/4 of the S mass was located in the higher altitude part of the aerosol layer, west of La Réunion  
178 (Fig. 4a; Methods, Section 3). Leading up to the eruptions (i.e., on Jan. 10), the S burden in  
179 background eH<sub>2</sub>SO<sub>4</sub> aerosol was < 0.001 Tg S. This result suggests that rapid aerosol conversion  
180 took place: within ~ 19 days, all the SO<sub>2</sub> released from the eruptions, corresponding to as much  
181 as 0.18 Tg S (8), was oxidized and converted to particles ( $\geq 140$  nm). By tracking the  
182 accumulation of S in eH<sub>2</sub>SO<sub>4</sub> aerosol, we calculate the average  $\tau_{\text{strat}}$  as ~ 10 – 13 days in the plume  
183 (see Methods, Section 4; Fig. 4b). We note, however, that if a sizeable fraction (e.g., 0.09 Tg) of  
184 the aerosol mass were not composed of H<sub>2</sub>SO<sub>4</sub>, this would yield a longer estimated  $\tau_{\text{strat}}$  (~ 14 –  
185 17 days) given the same SO<sub>2</sub> injection. A short  $\tau_{\text{strat}}$ , compared with the typical value of one  
186 month under climatological stratospheric conditions, helps explain the rapid production of large  
187 particles in the HT-HH plume and signals greater availability of the hydroxyl radical to react  
188 with methane and trace gases in the stratosphere (12, 22, 23).

## 189 190 **Discussion**

191 A rapid response to large or unusual volcanic eruptions with in situ observations can  
192 provide insight into the resulting aerosol microphysics, complement space-based aerosol  
193 retrievals (7, 8, 10), and be essential to evaluate models. Together with satellite retrievals of  
194 sAOD, POPS vertical profiles of particle size distributions enable the calculation of the aerosol  
195 layer's S mass and the mean  $\tau_{\text{strat}}$  of SO<sub>2</sub>. We determined that eH<sub>2</sub>SO<sub>4</sub> formation was complete  
196 within three weeks, which is consistent with a maximum effective radius (> 0.4  $\mu\text{m}$ ) observed in  
197 early February (Fig. S2). In situ measurements of SO<sub>2</sub> and eH<sub>2</sub>SO<sub>4</sub> and calculations of the aerosol  
198 layer's eH<sub>2</sub>SO<sub>4</sub> mass provide evidence that the bulk of the total S was injected above 25 km,  
199 which cannot be easily deduced from satellite retrievals of SO<sub>2</sub> and aerosol extinction (8, 10).  
200 These observations also indicate that SO<sub>2</sub> oxidation and aerosol conversion occurred at varying  
201 rates within the plume, corresponding to localized H<sub>2</sub>O enhancements. Radiosonde  
202 measurements confirm that H<sub>2</sub>O mixing ratios within the plume spanned more than an order of  
203 magnitude (< 100 ppmv to > 1000 ppmv) (9). Climatological lower stratospheric mixing ratios in  
204 the tropics do not typically exceed 4-5 ppmv (24). SO<sub>2</sub> oxidation and aerosol conversion took  
205 place ~ 3 times faster, on average, than under climatological stratospheric conditions. SO<sub>2</sub>  
206 oxidation accelerates substantially in the presence of H<sub>2</sub>O enhancements (12, 22, 23, 25). A short  
207  $\tau_{\text{strat}}$  of SO<sub>2</sub> reflects the heightened oxidative capacity of the atmosphere, with important  
208 implications on stratospheric chemistry and composition.

209 Our measurements clarify the contributions to aerosol extinction from H<sub>2</sub>O after the HT-  
210 HH eruptions, which has spurred discussion in the scientific community (10–13). We caution  
211 against conflating a response in the aerosol extinction with a similar change in aerosol mass for  
212 two reasons: H<sub>2</sub>O contributed ~30% to aerosol extinction in the fresh HT-HH plume. Light  
213 scattering efficiency is closely related to aerosol size, with a maximum efficiency (per unit  
214 volume) at 500 nm diameter (20). Due to the 560 nm diameter mode of the measured aerosol size  
215 distribution mode, the HT-HH aerosol layer resulted in a high sAOD relative to its injected mass.  
216 Radiosonde measurements show similarly elevated H<sub>2</sub>O throughout the plume between Jan. 20  
217 and Feb. 1 (one quarter of the observations between 26 – 28 km altitude from all vertical profiles  
218 during this period had  $7 \leq \text{H}_2\text{O} \leq 130$  ppmv) (26), signifying widespread implications for  
219  $\text{H}_2\text{SO}_4$  particle size and the S mass in the higher altitude part of the aerosol layer. Particle size  
220 distributions show that differences in the peak and shape of the size distribution result in  
221 substantial differences in aerosol extinction (e.g., Fig. 1). Questions remain about how H<sub>2</sub>O and  
222 other compounds reaching the stratosphere during an eruption might influence aerosol  
223 microphysics, including the propensity for new particle formation, condensation onto existing  
224 particles, and particle coagulation.

225 TR<sup>2</sup>Ex serves as a roadmap for future rapid response campaigns to volcanic eruptions and  
226 other stratospheric perturbations. Campaigns such as TR<sup>2</sup>EX further the understanding of aerosol  
227 processes in the stratosphere and inform models predicting climate impacts under a variety of  
228 past and potential future conditions. Stratospheric aerosol injection (SAI), one proposed method  
229 of climate intervention, would entail a large anthropogenic addition of stratospheric aerosol. The  
230 suite of instruments described here is capable of identifying potential SAI implementations,  
231 providing insight into the aerosol composition (i.e., sulfate or other) and hygroscopic effect, and  
232 could enable quantifying the mass (and altitude) of SAI.

233

## 234 **Methods**

### 235 1. Rapid Response Overview

236 POPS in situ observations (18) of aerosol size distributions were made as part of the  
237 National Oceanic and Atmospheric Administration (NOAA) Earth Radiation Budget program's  
238 Baseline Balloon Stratospheric Aerosol Profiles (B<sup>2</sup>SAP) project (27). The B<sup>2</sup>SAP project  
239 combines intensive periods of operation (IOP) with routine baseline measurements in the  
240 northern and southern hemispheres. For the Tonga volcano Rapid Response Experiment (TR<sup>2</sup>Ex)  
241 between Jan. 21 and Jan. 26, B<sup>2</sup>SAP IOP activities were coordinated with additional sonde and  
242 lidar measurements at the Maïdo Observatory (28) on La Réunion (21 °S, 55 °E). TR<sup>2</sup>Ex balloon  
243 payloads consisted of either: (A) a POPS, a sulfur dioxide (SO<sub>2</sub>) sonde, an Electrochemical  
244 Concentration Cell (ECC) ozonesonde and a radiosonde, or (B), an ECC ozonesonde, a Compact  
245 Optical Back-scatter Aerosol Detector (COBALD) instrument and a radiosonde (Table S1;  
246 COBALD, ozonesonde, and lidar measurements are discussed elsewhere (19). The ground-based  
247 lidars and the COBALD provided information on aerosol extinction (18) and backscattering,  
248 respectively. Unfortunately, quantitative information on the aerosol depolarization in the plume  
249 during TR<sup>2</sup>Ex does not exist because the lidar at the Maïdo observatory was not calibrated for  
250 depolarization. Subsequent POPS and NOAA Frost point Hygrometer (FPH) launches in  
251 February, March, and June 2022 at the Maïdo Observatory were part of what are now routine  
252 B<sup>2</sup>SAP soundings (Table S1) (27).

253 SO<sub>2</sub> sonde (14) measurements have lower uncertainty and considerably better vertical  
254 resolution than satellite SO<sub>2</sub> retrievals (8), particularly after an energetic volcanic eruption. A

255 modified ECC ozonesonde, the SO<sub>2</sub> sonde removes ozone from the sample prior to detection  
256 using a filter, allowing stratospheric as well as tropospheric SO<sub>2</sub> to be quantified using pre-flight  
257 calibrations (14). The SO<sub>2</sub> sonde has a ~ 25 sec response time, similar to that of an ozonesonde.  
258 SO<sub>2</sub> data (Fig. 2) reflect a correction for this time (and altitude) lag (29, 30). CFH (31) and FPH  
259 (16) instruments measuring H<sub>2</sub>O were used to calculate ambient particle size, and Ozone  
260 Mapping and Profiler Suite-Limb Profile (OMPS-LP) retrievals (17) were used to calculate the  
261 volcanic plume's aerosol burden, as described below.

262

## 263 2. The POPS measurements and inherent assumptions

264 Particle sizing inherently requires assumptions about particle morphology and refractive  
265 index related to aerosol composition (18). Here, we assume that particles are spherical and  
266 composed of sulfuric acid (H<sub>2</sub>SO<sub>4</sub>) and water, with a corresponding refractive index of 1.45 at  
267 405 nm (the wavelength of the POPS laser), leading to a reported particle number and size  
268 distribution between 140 nm – 2.5 μm in diameter. Telemetered data are quality assured based  
269 on available engineering parameters, including the instrument temperature, measured with a  
270 thermistor located on the POPS laminar flow element, and the instrument flow (27). Particles are  
271 expected to be at (or close to) equilibrium with the instrument temperature at the time of  
272 detection, given a particle transit time of 60 – 90 ms. We note that POPS particle transit times  
273 exceeded modeled timescales required for aerosol growth or evaporation within the plume, in  
274 line with similar calculations from Kovilakam and Deshler (32) and Jonsson et al. (33).

275 The S in the eH<sub>2</sub>SO<sub>4</sub> aerosol column mass and mass mixing ratios are calculated from the  
276 measured aerosol size distribution and particle density. The aerosol weight (wt.%) eH<sub>2</sub>SO<sub>4</sub> can be  
277 determined using the partial pressure of H<sub>2</sub>O at a range of temperatures (34–37). We apply the  
278 formulation of Tabazedah et al. (37), which is suitable for low temperatures observed in the  
279 lower stratosphere (when eH<sub>2</sub>SO<sub>4</sub> ≤ 80 wt. %) and is based on Steele and Hamill (35), and the  
280 expression of Gmitro and Vermeulen when eH<sub>2</sub>SO<sub>4</sub> > 80 wt. % (34). In the stratosphere,  
281 particles have a calculated ≥ 80% wt% eH<sub>2</sub>SO<sub>4</sub> at the time of detection due to instrument  
282 temperatures (268 – 278 K) that are considerably higher than ambient stratospheric air (ΔT = 50  
283 – 75 K). Particle density at the time of detection is both wt.% and temperature dependent (38–  
284 40). We use two parameterizations valid for temperatures between 233 – 298 K given different  
285 wt. % (39, 40).

286 Ambient particle diameter is calculated according to Steele and Hamill (35) from the  
287 measured (dehydrated) particle diameter, the particle wt. % and density both at the time of  
288 detection and in ambient air, assuming that the particle was at equilibrium in both cases, and that  
289 only water (not H<sub>2</sub>SO<sub>4</sub>) was lost from the particle during sampling (Fig. S2a). Measured aerosol  
290 size distributions were averaged into 100 m altitude bins, to improve counting statistics and  
291 facilitate the requisite merges with frost point hygrometer data from other launches. Possible  
292 errors in measured particle sizing are driven primarily by Mie resonances (18). Uncertainty in  
293 H<sub>2</sub>O (<=6%), air temperature (< 1%), and uncertainties in the parameterizations of the wt. % and  
294 density contribute additionally to possible errors in calculated ambient sizing (Fig. S2), and the  
295 calculated S in eH<sub>2</sub>SO<sub>4</sub> mass mixing ratios and column mass (Fig. 2).

296 As in situ size distribution measurements provide no information on aerosol composition,  
297 we cannot rule out the possibility that aerosol could have consisted of ash or some other material,  
298 such as sea salt, coated (or internally mixed) with H<sub>2</sub>SO<sub>4</sub>. Contributions from HNO<sub>3</sub> aerosol or  
299 mixtures containing HNO<sub>3</sub> and H<sub>2</sub>SO<sub>4</sub> were considered but dismissed based on equilibrium  
300 calculations (33, 41, 42). Although volcanic lightning on Jan. 15 (43) may have injected NO



301 directly into the stratosphere,  $\text{HNO}_3$  hardly condenses at temperatures  $\geq 220$  K observed in the  
302 plume, despite large enhancements in stratospheric  $\text{H}_2\text{O}$ .

303 The assumptions made here regarding particle composition and morphology are  
304 supported by space-based Cloud-Aerosol Lidar with Orthogonal Polarization (CALIOP)  
305 retrievals and geostationary satellite RGB-Ash composite imagery within the first few days of  
306 the HT-HH eruption on Jan. 15 (11). CALIOP retrievals showed particles with low  
307 depolarization, indicating spherical  $\text{H}_2\text{SO}_4$  particles moving westward towards La Réunion on  
308 Jan. 20. The geostationary satellite RGB-Ash composite images depicted a concomitant light  
309 green  $\text{SO}_2$  plume (with little to no ash) during this period.

310

### 311 3. Calculating the aerosol column and plume S burden

312 Vertical profiles of aerosol extinction at 997 nm, corresponding to the native wavelength  
313 of the OMPS-LP sensor, are calculated using publicly available Mie codes (44, 45) and the  
314 calculated particle size distribution in ambient air. POPS stratospheric ambient aerosol optical  
315 depth (sAOD) is the sum of calculated ambient aerosol extinction above the tropopause.  
316 Similarly, the POPS stratospheric S column in  $\text{eH}_2\text{SO}_4$  aerosol ( $\text{g S m}^{-2}$ ) at a single geographic  
317 location is quantified as the sum of the S in  $\text{eH}_2\text{SO}_4$  aerosol ( $\mu\text{g S m}^{-2}$  air) in each 100 m altitude  
318 bin above the tropopause. A baseline value of the S column in  $\text{eH}_2\text{SO}_4$  aerosol, calculated from a  
319 vertical profile outside the plume on Jan. 23 (14 UTC), was subtracted from each measurement  
320 that encountered the plume to determine the S in the aerosol layer ( $\text{g S m}^{-2}$ ). Because  $\text{SO}_2$   
321 measurements were below the  $\text{SO}_2$  sonde's limit of detection outside the plume, no similar  
322 subtraction of the S column in  $\text{SO}_2$  under baseline conditions was made following integration for  
323 comparisons in Figure 2d.

324 A linear regression between the POPS calculated ambient sAOD and S in  $\text{eH}_2\text{SO}_4$  column  
325 mass enables global retrievals of OMPS-LP sAOD to be used to infer the S column mass across  
326 the entire aerosol layer and track the S aerosol burden as the plume evolves. Estimates of the  
327  $\text{eH}_2\text{SO}_4$  aerosol layer mass, based on relationships between the POPS measured (dehydrated)  
328 sAOD and POPS stratospheric S column ( $\pm$  uncertainty) and the calculated ambient sAOD and  
329 POPS stratospheric S column ( $\pm$  uncertainty) over La Réunion between Jan. 22 and Jun. 9 are  
330 shown in Figure S4a. The reported uncertainty in OMPS-LP sAOD signal in the stratosphere  
331 (10% at  $\lambda = 997$  nm) (17) is negligible compared to the differences in the slope and intercept  
332 POPS sAOD vs. mass relationships (Fig. S4a). We note that recent debate with respect to  
333 potential OMPS-LP retrieval biases (46) is beyond the scope of this work but would lead to a  
334 lower  $\text{eH}_2\text{SO}_4$  aerosol layer mass. The maximum value of daily sAOD from the OMPS-LP sensor  
335 on Jan. 10 (50°S – 50°N) was used as the sAOD threshold to identify the geographic extent of  
336 the tropical HT-HH aerosol layer (Fig. S4b); its median (0.0025) was used as a background  
337 sAOD value in the tropics. The linear relationships from Fig. S4a were applied to each daily  
338 sAOD value in the aerosol layer to infer the S column ( $\text{g S m}^{-2}$ ) in each ( $2^\circ$  latitude x  $24^\circ$   
339 longitude) grid cell. The resulting S column using the relationship between the ambient sAOD  
340 and S in  $\text{eH}_2\text{SO}_4$  column mass is shown in Figure 3. For reference, the  $\text{H}_2\text{O}$  plume extent,  
341 calculated from MLS retrieval levels between 10 and 46 hPa using MLS  $\text{H}_2\text{O}$  anomalies between  
342 Jan. 21 – Jan. 23 (defined as the median  $\pm 3$  x the mean absolute deviation) is also shown in  
343 Figure 3c, compared to the aerosol layer.

344 The S column was then multiplied by the area of the corresponding geographic grid cell  
345 ( $\text{m}^2$ ) and summed to determine the total stratospheric S burden (Tg S) over that area. By  
346 applying the relationships from Fig. S4a to the background sAOD value, multiplied by the

347 aerosol layer's geographic area, we similarly calculated the corresponding S burden under  
 348 background conditions in each case. The S burden under background conditions was then  
 349 subtracted from the total stratospheric aerosol S burden to yield the volcanic aerosol layer's S  
 350 burden  $\pm$  uncertainty (Tg S) shown in Figure 4. The uncertainty in the S burden (the shaded  
 351 black region) reflects the range of the estimates shown in Figure S4a. The S mass in the upper  
 352 part of the plume was approximated as the sum of the S burden (in  $e\text{H}_2\text{SO}_4$  aerosol) west of La  
 353 Réunion ( $55^\circ$  E), when the higher altitude part of the aerosol layer was last observed on Jan. 23  
 354 00 UTC (Fig. 1d)(19). La Réunion is located near the latitudinal edge ( $48^\circ$  E) of two adjacent  
 355 OMPS-LP grid-cells. Thus, this estimate represents the arithmetic mean  
 356 ( $\pm$  the standard deviation) of the S burden in the adjacent OMPS-LP grid cells centered at  $36^\circ$   
 357 E and  $60^\circ$  E (Fig. 4).  
 358

#### 359 4. Estimating the $\text{SO}_2$ lifetime

360 By monitoring the aerosol loading following an eruption, we can estimate the initial  
 361 injection of S and subsequently deduce the stratospheric lifetime ( $\tau_{\text{strat}}$ ) of  $\text{SO}_2$ . We assume that  
 362 all the  $\text{SO}_2$  is converted to  $\text{H}_2\text{SO}_4$ :  
 363

$$364 \quad 1. \frac{d[\text{H}_2\text{SO}_4]}{dt} = -\frac{d[\text{SO}_2]}{dt}, \text{ and } [\text{SO}_2] = [\text{SO}_2_{t=0}] - ([\text{H}_2\text{SO}_4] - [\text{H}_2\text{SO}_4_{t=0}])$$

366 Making these substitutions into the first order rate law  $\frac{d[\text{SO}_2]}{[\text{SO}_2]} = -kdt$  and integrating  
 367 demonstrates that the amount of  $\text{H}_2\text{SO}_4$  produced depends on the initial injection of  $\text{SO}_2$  and on  
 368 the background  $\text{H}_2\text{SO}_4$  burden (together with any initial injection of aerosol) and enables us to  
 369 calculate  $\tau_{\text{strat}}$  of  $\text{SO}_2$  through linear regression against  $t$  (elapsed days since 4:00 UTC on Jan.  
 370 15), where  $k$  is the slope of the line and  $\tau_{\text{strat}} = 1/k$ :  
 371

$$372 \quad 2. \ln \frac{[\text{SO}_2_{t=0}]}{[\text{SO}_2_{t=0}] - ([\text{H}_2\text{SO}_4] - [\text{H}_2\text{SO}_4_{t=0}])} = kt$$

373 The initial injection of S,  $\text{SO}_2_{t=0}$ , is based on satellite retrievals of  $\text{SO}_2$ , which are slightly greater  
 374 than the maximum accrual of S in  $e\text{H}_2\text{SO}_4$  aerosol after the eruption (0.190 Tg; Fig. 4a).  $\tau_{\text{strat}}$  was  
 375 calculated using a range of values for the initial  $\text{SO}_2$  injection (0.195 – 0.215 Tg S in  $\text{SO}_2$ ). Prior  
 376 to the eruption (e.g, on Jan. 10), the initial S burden in the aerosol layer is close to zero (0.0005  
 377 Tg S in  $e\text{H}_2\text{SO}_4$ ), which is used as the value for  $\text{H}_2\text{SO}_4_{t=0}$ . If as much as 0.09 Tg of aerosol mass  
 378 were not composed of  $\text{H}_2\text{SO}_4$  (0.03 Tg S is in 0.09 Tg  $e\text{H}_2\text{SO}_4$ ) this would result in an estimated  
 379  $\tau_{\text{strat}}$  of 15-17 days. Equation 2 ignores a potential time lag required for either particle formation  
 380 or aerosol growth through condensation to particle diameter  $\geq 0.14 \mu\text{m}$  from  $\text{H}_2\text{SO}_4$  gas,  
 381 considered negligible in this case.  
 382  
 383

#### 384 Data Availability

385 The processed POPS aerosol size distribution data from all launches used in this study  
 386 may be found under the supporting data tab for this manuscript at  
 387 <https://csl.noaa.gov/projects/b2sap/data.html>, where processed  $\text{SO}_2$  and  $\text{H}_2\text{O}$  data from TR<sup>2</sup>Ex,  
 388 and processed daily files of OMPS-LP sAOD and MLS  $\text{H}_2\text{O}$  plume areas and anomalies from 21  
 389 hPa are also available. Raw OMPS-LP and MLS  $\text{H}_2\text{O}$  data may be found at

390 [https://disc.gsfc.nasa.gov/datasets/OMPS\\_NPP\\_LP\\_L2\\_AER\\_DAILY\\_2/summary](https://disc.gsfc.nasa.gov/datasets/OMPS_NPP_LP_L2_AER_DAILY_2/summary) and  
391 [https://disc.gsfc.nasa.gov/datasets/ML2H2O\\_004/summary?keywords=aura](https://disc.gsfc.nasa.gov/datasets/ML2H2O_004/summary?keywords=aura), respectively. Code  
392 is publicly available at <https://github.com/elizabethasher/hthhPY>.

393

### 394 **Funding Information**

395 This work was supported by the National Oceanic and Atmospheric Administration  
396 (NOAA) Earth Radiation Budget program. The authors acknowledge the European  
397 Communities, the Région Réunion, CNRS, and Université de la Réunion for their support and  
398 contributions in the construction phase of the research infrastructure OPAR (Observatoire de  
399 Physique de l'Atmosphère de La Réunion, including Maïdo Observatory). OPAR is presently  
400 funded by CNRS (INSU), Météo France, and Université de La Réunion and managed by OSU- R  
401 (Observatoire des Sciences de l'Univers de La Réunion, UAR 3365). Development,  
402 maintenance, and analysis of the OMPS-LP aerosol product are supported by the NASA Earth  
403 Science TASNPP (grant # 80NSSC18K0847) and SNPPSP (grant # 80NSSC22K0157)  
404 programs. Opinions, findings and conclusions contained herein reflect the authors' views, not  
405 those of NOAA.

406

### 407 **Open Access**

408 An open access license has not been selected.

409

### 410 **Competing interests**

411 The authors declare no competing financial interests.

412

### 413 **Materials and Correspondence**

414 Corresponding author, Elizabeth Asher ([Elizabeth.asher@noaa.gov](mailto:Elizabeth.asher@noaa.gov)) should be contacted  
415 with any questions or requests for material.

416

417

### 418 **References**

419

- 420 1. S. Solomon, *et al.*, The Persistently Variable “Background” Stratospheric Aerosol Layer  
421 and Global Climate Change. *Science* **333**, 866–870 (2011).
- 422 2. A. Feinberg, *et al.*, Improved tropospheric and stratospheric sulfur cycle in the aerosol–  
423 chemistry–climate model SOCOL-AERv2. *Geosci. Model Dev.* **12**, 3863–3887 (2019).
- 424 3. M. H. Hitchman, M. McKay, C. R. Trepte, A climatology of stratospheric aerosol. *J.*  
425 *Geophys. Res.* **99**, 20689 (1994).
- 426 4. S. Kremser, *et al.*, Stratospheric aerosol-Observations, processes, and impact on climate:  
427 Stratospheric Aerosol. *Rev. Geophys.* **54**, 278–335 (2016).
- 428 5. L. O. Muser, *et al.*, Particle aging and aerosol–radiation interaction affect volcanic plume  
429 dispersion: evidence from the Raikoke 2019 eruption. *Atmospheric Chem. Phys.* **20**, 15015–  
430 15036 (2020).

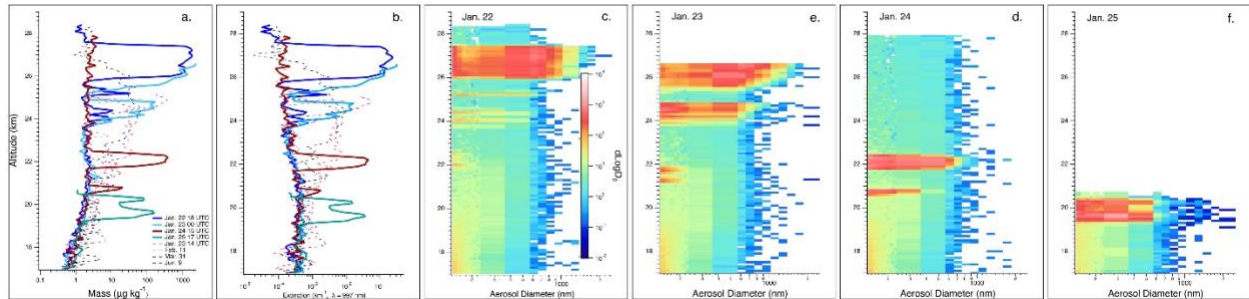
- 431 6. C. J. Wright, *et al.*, Surface-to-space atmospheric waves from Hunga Tonga–Hunga  
432 Ha’apai eruption. *Nature* **609**, 741–746 (2022).
- 433 7. L. Millán, *et al.*, The Hunga Tonga-Hunga Ha’apai Hydration of the Stratosphere. *Geophys.*  
434 *Res. Lett.* **49** (2022).
- 435 8. S. A. Carn, N. A. Krotkov, B. L. Fisher, C. Li, Out of the blue: Volcanic SO<sub>2</sub> emissions  
436 during the 2021–2022 eruptions of Hunga Tonga—Hunga Ha’apai (Tonga). *Front. Earth*  
437 *Sci.* **10**, 976962 (2022).
- 438 9. H. Vömel, S. Evan, M. Tully, Water vapor injection into the stratosphere by Hunga Tonga-  
439 Hunga Ha’apai. *Science* **377**, 1444–1447 (2022).
- 440 10. G. Taha, *et al.*, Tracking the 2022 Hunga Tonga-Hunga Ha’apai aerosol cloud in the upper  
441 and middle stratosphere using space-based observations. *Geophys. Res. Lett.* (2022)  
442 <https://doi.org/10.1029/2022GL100091> (October 2, 2022).
- 443 11. B. Legras, *et al.*, The evolution and dynamics of the Hunga Tonga–Hunga Ha’apai sulfate  
444 aerosol plume in the stratosphere. *Atmospheric Chem. Phys.* **22**, 14957–14970 (2022).
- 445 12. Y. Zhu, *et al.*, Perturbations in stratospheric aerosol evolution due to the water-rich plume  
446 of the 2022 Hunga-Tonga eruption. *Commun. Earth Environ.* **3**, 248 (2022).
- 447 13. M. R. Schoeberl, *et al.*, Analysis and Impact of the Hunga Tonga-Hunga Ha’apai  
448 Stratospheric Water Vapor Plume. *Geophys. Res. Lett.* **49** (2022).
- 449 14. S. Yoon, *et al.*, Development and testing of a novel sulfur dioxide sonde. *Atmospheric*  
450 *Meas. Tech.* **15**, 4373–4384 (2022).
- 451 15. H. Vömel, T. Naebert, R. Dirksen, M. Sommer, An update on the uncertainties of water  
452 vapor measurements using cryogenic frost point hygrometers. *Atmospheric Meas. Tech.* **9**,  
453 3755–3768 (2016).
- 454 16. E. G. Hall, *et al.*, Advancements, measurement uncertainties, and recent comparisons of the  
455 NOAA frost point hygrometer. *Atmospheric Meas. Tech.* **9**, 4295–4310 (2016).
- 456 17. G. Taha, *et al.*, OMPS LP Version 2.0 multi-wavelength aerosol extinction coefficient  
457 retrieval algorithm. *Atmospheric Meas. Tech.* **14**, 1015–1036 (2021).
- 458 18. R. S. Gao, *et al.*, A light-weight, high-sensitivity particle spectrometer for PM<sub>2.5</sub> aerosol  
459 measurements. *Aerosol Sci. Technol.* **50**, 88–99 (2016).
- 460 19. A. Baron, *et al.*, Early Evolution of the Stratospheric Aerosol Plume Following the 2022  
461 Hunga Tonga-Hunga Ha’apai Eruption: Lidar Observations From Reunion (21°S, 55°E).  
462 *Geophys. Res. Lett.* **50**, e2022GL101751 (2023).

- 463 20. D. M. Murphy, *et al.*, Radiative and chemical implications of the size and composition of  
464 aerosol particles in the existing or modified global stratosphere. *Atmospheric Chem. Phys.*  
465 **21**, 8915–8932 (2021).
- 466 21. M. Höpfner, *et al.*, Sulfur dioxide (SO<sub>2</sub>) from MIPAS in the upper troposphere and lower  
467 stratosphere 2002–2012. *Atmospheric Chem. Phys.* **15**, 7017–7037 (2015).
- 468 22. A. N. LeGrande, K. Tsigaridis, S. E. Bauer, Role of atmospheric chemistry in the climate  
469 impacts of stratospheric volcanic injections. *Nat. Geosci.* **9**, 652–655 (2016).
- 470 23. J. H. Seinfeld, Pandis, Spyros N., *Atmospheric Chemistry and Physics: From Air Pollution*  
471 *to Climate Change* (John Wiley & Sons, 2006).
- 472 24. D. F. Hurst, *et al.*, Recent divergences in stratospheric water vapor measurements by frost  
473 pointhygrometers and the Aura Microwave Limb Sounder. *Atmospheric Meas. Tech.* **9**,  
474 4447–4457 (2016).
- 475 25. Y. Zhu, *et al.*, Persisting volcanic ash particles impact stratospheric SO<sub>2</sub> lifetime and  
476 aerosol optical properties. *Nat. Commun.* **11**, 4526 (2020).
- 477 26. Vömel, Holger, Hunga Tonga-Hunga Ha’apai stratospheric water vapor from Vaisala RS41  
478 radiosondes <https://doi.org/10.5065/P328-Z959> (September 25, 2022).
- 479 27. M. A. Todt, *et al.*, Baseline Balloon Stratospheric Aerosol Profiles (B<sup>2</sup> SAP)- Systematic  
480 measurements of aerosol number density and size. *J. Geophys. Res. Atmospheres*,  
481 e2022JD038041 (2023).
- 482 28. A. Baron, *et al.*, “Early evolution of the Hunga &#8211; Tonga Volcanic Plume from Lidar  
483 Observations at Reunion Island (Indian Ocean, 21&#176;S, 55&#176;E)” (display, 2022)  
484 <https://doi.org/10.5194/egusphere-egu22-13599> (February 5, 2023).
- 485 29. H. Vömel, *et al.*, A new method to correct the electrochemical concentration cell (ECC)  
486 ozonesonde time response and its implications for “background current” and pump  
487 efficiency. *Atmospheric Meas. Tech.* **13**, 5667–5680 (2020).
- 488 30. L.-J. Huang, M.-J. Chen, C.-H. Lai, H.-T. Hsu, C.-H. Lin, New Data Processing Equation to  
489 Improve the Response Time of an Electrochemical Concentration Cell (ECC) Ozonesonde.  
490 *Aerosol Air Qual. Res.* **15**, 935–944 (2015).
- 491 31. H. Vömel, D. E. David, K. Smith, Accuracy of tropospheric and stratospheric water vapor  
492 measurements by the cryogenic frost point hygrometer: Instrumental details and  
493 observations. *J. Geophys. Res.* **112**, D08305 (2007).
- 494 32. M. Kovilakam, T. Deshler, On the accuracy of stratospheric aerosol extinction derived from  
495 in situ size distribution measurements and surface area density derived from remote SAGE  
496 II and HALOE extinction measurements. *J. Geophys. Res. Atmospheres* **120**, 8426–8447  
497 (2015).

- 498 33. H. H. Jonsson, *et al.*, Performance of a Focused Cavity Aerosol Spectrometer for  
499 Measurements in the Stratosphere of Particle Size in the 0.06–2.0- $\mu\text{m}$ -Diameter Range. *J.*  
500 *Atmospheric Ocean. Technol.* **12**, 115–129 (1995).
- 501 34. J. I. Gmitro, T. Vermeulen, Vapor-liquid equilibria for aqueous sulfuric acid. *AIChE J.* **10**,  
502 740–746 (1964).
- 503 35. H. M. Steele, P. Hamill, Effects of temperature and humidity on the growth and optical  
504 properties of sulphuric acid–water droplets in the stratosphere. *J. Aerosol Sci.* **12**, 517–528  
505 (1981).
- 506 36. S. L. Clegg, P. Brimblecombe, Application of a Multicomponent Thermodynamic Model to  
507 Activities and Thermal Properties of 0–40 mol kg<sup>-1</sup> Aqueous Sulfuric Acid from <200 to  
508 328 K. *J. Chem. Eng. Data* **41**, 1530–1530 (1996).
- 509 37. A. Tabazadeh, O. B. Toon, S. L. Clegg, P. Hamill, A new parameterization of H<sub>2</sub>SO<sub>4</sub>/H<sub>2</sub>  
510 O aerosol composition: Atmospheric implications. *Geophys. Res. Lett.* **24**, 1931–1934  
511 (1997).
- 512 38. E. Washburn W., Ed., *International critical tables of numerical data, physics, chemistry*  
513 *and technology* (McGraw-Hill, 1928).
- 514 39. M. Kulmala, A. Laaksonen, L. Pirjola, Parameterizations for sulfuric acid/water nucleation  
515 rates. *J. Geophys. Res. Atmospheres* **103**, 8301–8307 (1998).
- 516 40. L. Oca, J. M. Campillo-Robles, M. M. Bou-Ali, Review and Analysis of Thermophysical  
517 Properties of a Sulfuric Acid–Water Electrolyte. *J. Chem. Eng. Data* **63**, 3572–3583 (2018).
- 518 41. M. D. Petters, S. M. Kreidenweis, A single parameter representation of hygroscopic growth  
519 and cloud condensation nucleus activity. *Atmospheric Chem. Phys.* **7**, 1961–1971 (2007).
- 520 42. Jack Alf Goff, S. Gratch, Low-pressure properties of water from -160 to 212 °F in  
521 (Transactions of the American Society of Heating and Ventilating Engineers, 1946), pp.  
522 95–122.
- 523 43. D. A. Yuen, *et al.*, Under the surface: Pressure-induced planetary-scale waves, volcanic  
524 lightning, and gaseous clouds caused by the submarine eruption of Hunga Tonga-Hunga  
525 Ha’apai volcano. *Earthq. Res. Adv.* **2**, 100134 (2022).
- 526 44. C. F. Bohren, D. R. Huffman, *Absorption and Scattering of Light by Small Particles*, 1st  
527 Ed. (Wiley, 1998) <https://doi.org/10.1002/9783527618156> (September 23, 2022).
- 528 45. B. J. Sumlin, W. R. Heinson, R. K. Chakrabarty, Retrieving the aerosol complex refractive  
529 index using PyMieScatt: A Mie computational package with visualization capabilities. *J.*  
530 *Quant. Spectrosc. Radiat. Transf.* **205**, 127–134 (2018).
- 531 46. A. E. Bourassa, *et al.*, Tomographic Retrievals of Hunga Tonga-Hunga Ha’apai Volcanic  
532 Aerosol. *Geophys. Res. Lett.* **50** (2023).

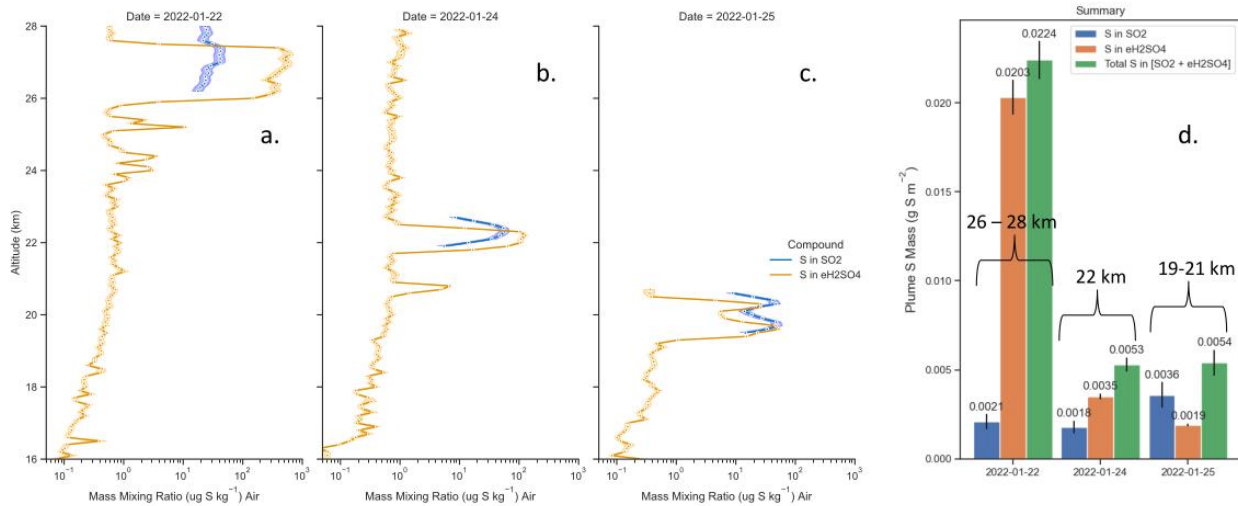
533  
534  
535  
536  
537

**Figures**



538  
539  
540  
541  
542  
543  
544  
545  
546

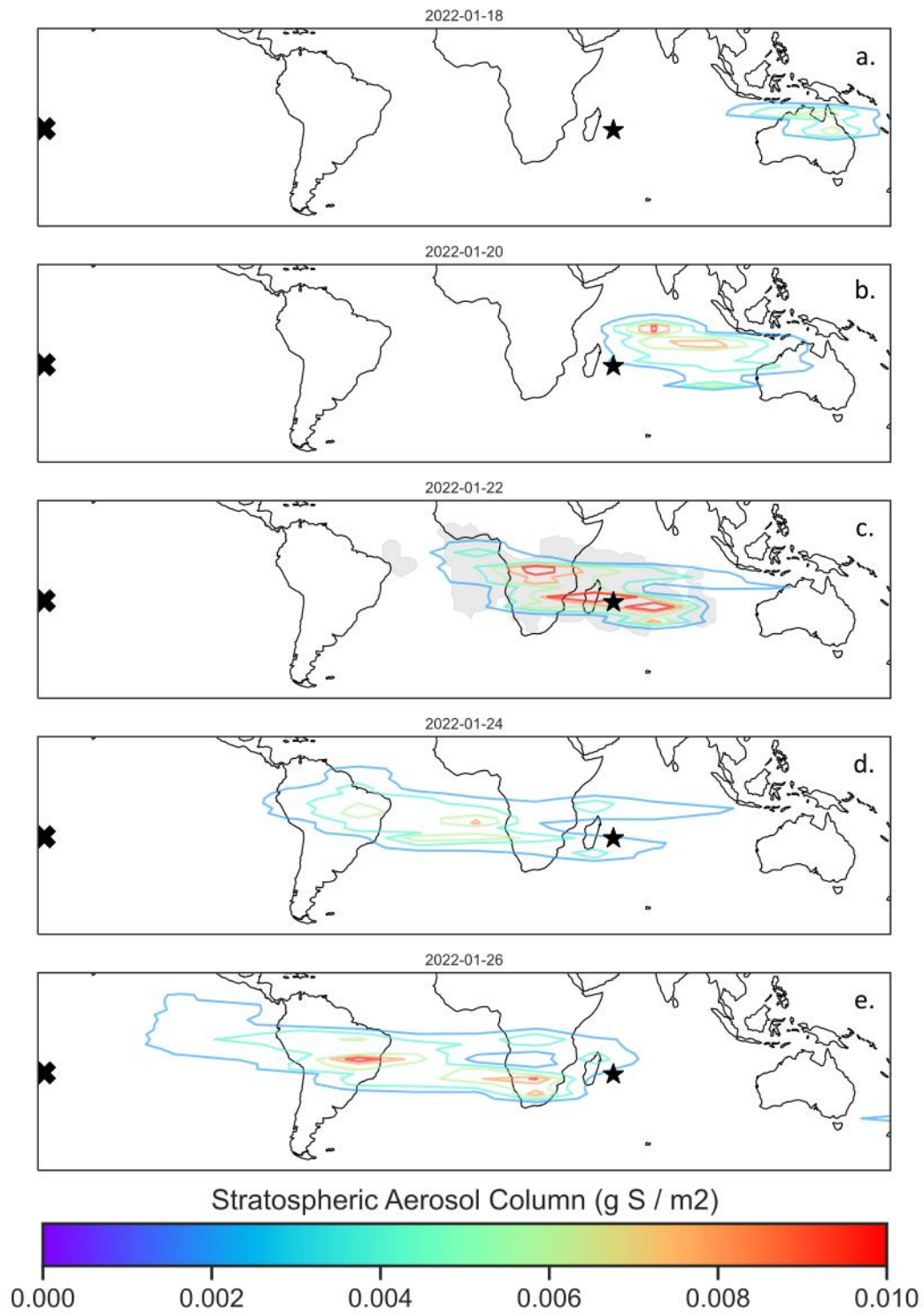
**Figure 1.** Vertical profiles of calculated bulk aerosol properties between January and June 2022 (from POPS size distribution data), including mass mixing ratios (a) and ambient extinction using Steele and Hamill (35)(b), both of which use the legend in panel (a), and vertical profiles of the measured aerosol size distributions from TR<sup>2</sup>Ex launches when the fresh HT-HH aerosol plume was encountered (c, d, e, f). Aerosol size distributions (dN/dLogD<sub>p</sub>) for the four TR<sup>2</sup>Ex soundings (c, d, e, f) use the color scale in panel (c).



547  
548  
549  
550  
551  
552  
553  
554

**Figure 2.** On three different dates, vertical profiles of S in SO<sub>2</sub> mass mixing ratios and calculated S in eH<sub>2</sub>SO<sub>4</sub> mass mixing ratios based on aerosol size distributions, when both instruments measured the volcanic plume with low uncertainties (a-c), and a summary of the S column mass in SO<sub>2</sub>, the S column mass in eH<sub>2</sub>SO<sub>4</sub>, and the total S column mass ([S in SO<sub>2</sub>] + [S in eH<sub>2</sub>SO<sub>4</sub>]) observed within the plume (d). Shaded areas and error bars show the uncertainty in SO<sub>2</sub> sonde measurements ( $\leq 20\%$ ) and the uncertainty in calculated eH<sub>2</sub>SO<sub>4</sub> mass mixing ratios and S mass including possible error related to aerosol sizing and aerosol density.





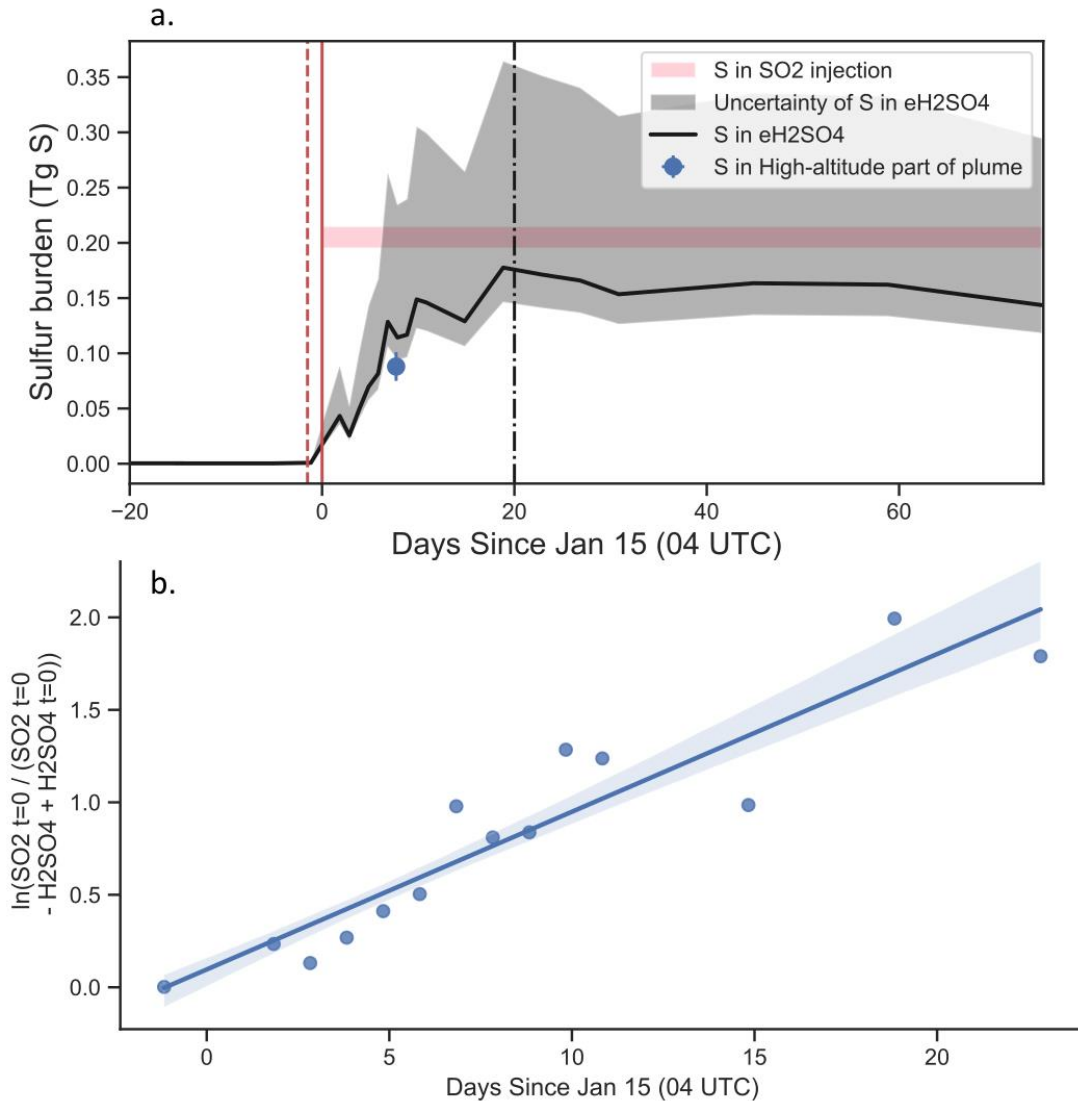
556

557 **Figure 3.** Contour plots of the  $\text{eH}_2\text{SO}_4$  aerosol column ( $\text{g m}^{-2}$ ), calculated using the equation in

558 the Fig. S4a caption, for 5 days from Jan. 18 to Jan 26 (a-e). On Jan. 22, the gray shaded area



559 shows the maximum plume extent between Jan. 21 – Jan. 23 as determined from MLS H<sub>2</sub>O  
 560 anomalies at 21 hPa. Locations of HT-HH and La Réunion are marked with a cross and star,  
 561 respectively.  
 562



563  
 564 **Figure 4.** A time series of the calculated S burden in eH<sub>2</sub>SO<sub>4</sub> aerosol, calculated using a  
 565 combination of POPS measurements and OMPS-LP retrievals (a) and the estimation of the  $\tau_{\text{strat}}$   
 566 (b). The calculated S burden in eH<sub>2</sub>SO<sub>4</sub> aerosol (black line) represents the relationship between  
 567 calculated ambient sAOD and the mass, and agrees with estimates of the S injected as SO<sub>2</sub> from  
 568 satellites (7, 8) (pink shaded region). The uncertainty (black shaded region) represents the range  
 569 of assumptions considered in Figure S4a. The approximated S mass in the higher altitude part of  
 570 the plume, west of La Réunion on Jan. 23 00 UTC is also shown. OMPS-LP Dashed vertical  
 571 lines depict the period of eH<sub>2</sub>SO<sub>4</sub> aerosol accumulation. The S burden from this period is used to  
 572 calculate the stratospheric lifetime of SO<sub>2</sub>,  $\tau_{\text{strat}} = 1/k$ , as shown in equation 3 (Methods

573 Section 3). Assuming an SO<sub>2</sub> injection of 0.205 Tg S in SO<sub>2</sub> (7, 8)  $k = 0.10$  ( $r^2 = 0.87$ ;  $p <$   
574  $1.23E-6$ ; 1 standard deviation of the slope is  $\pm 0.011$ ), suggesting a  $\tau_{\text{strat}}$  for SO<sub>2</sub> of  $\sim 10$  days (b).  
575